Astron. Astrophys. 345, 156–162 (1999)

ASTRONOMY AND ASTROPHYSICS

Microscopic diffusion and subdwarfs

P. Morel[1] **and A. Baglin**[2]

[1] Département Cassini, UMR CNRS 6529, Observatoire de la Côte d'Azur, BP 4229, F-06304 Nice Cedex 4, France
[2] DESPA, URA CNRS 264, Observatoire de Paris-Meudon, F-92195 Meudon Principal Cedex, France

Received 16 November 1998 / Accepted 4 February 1999

Abstract. The recent distance determinations by HIPPARCOS have allowed to locate very precisely a reasonable set of subdwarfs in the HR diagram. A detailed comparison with evolutionary models is now possible and it has been recently claimed that the observed lower part of the main-sequence is cooler than the computed one. In this paper we show that microscopic diffusion could be the physical explanation of such a systematic shift. We emphazise the fact that, as diffusion alters surface abundances, the initial metal content of the stellar material is higher than the present one. A "calibration" procedure is necessary when comparing observed and theoretical HR diagram, to take into account this effect.

Key words: diffusion – stars: Hertzsprung–Russel (HR) and C-M diagrams – stars: late-type

1. Introduction

Microscopic diffusion is a basic phenomenon, but, in the physical conditions of stellar interiors the small diffusion velocities imply long time scales to obtain significant modifications on the global parameters of real stars. To be efficient, the medium has to be quiet enough, so that large scale motion cannot prevent the settling. Acting essentially in radiative zones, it is now being advocated to explain a variety of observed facts, as lithium abundances in young and old population (Vauclair & Charbonnel 1998), abundances anomalies in different classes of young stars (Hui Bon Hao & Alecian 1998 and references herein), globular cluster evolution and age determination (Chaboyer et al. 1992). In the Sun, the insertion of microscopic diffusion in the modeling improves significantly the agreement between the theoretical and the "seismic" model (see e.g. Christensen-Dalsgaard et al. 1996; Richard et al. 1996; Morel et al. 1997; Brun et al. 1998). In the present state of art the computed sound speed, beneath the solar convection zone, agrees within a rms discrepancy better than 0.2% (Gough et al. 1996); the predicted values of the radius at the bottom of the convection zone and the helium abundance at the solar surface agree within the error bar with their values inferred from helioseismology (see e.g. Basu 1997).

Send offprint requests to: P. Morel
Correspondence to: Pierre.Morel@obs-nice.fr

Subdwarfs represent a clue in the general framework of stellar evolution in particular to estimate the globular clusters ages. A precise knowledge of their internal structure and of the stage of evolution is then badly needed.

As in such old objects the evolutionary time scale becomes of the same order as the diffusion one, significant effects due to this physical process are expected on their global properties.

Several papers have already mentioned the influence of microscopic diffusion in old objects (see e.g. Chaboyer et al. 1992; Mazitelli et al. 1995; Castellani et al. 1997), but focussed generally on the consequences on the age of the oldest globular clusters.

Up to now, the poor quality of the observed parameters of population II objects did not allow to refine their theory. The recent distance determinations of subdwarfs by HIPPARCOS (Perryman et al. 1997) has revolutionized the field. Combining these results with large improvement of effective temperature and bolometric corrections for low metal atmospheres (Alonso et al. 1996), a reasonable set of subdwarfs have been located very precisely in the HR diagram. A detailed comparison with evolutionary models is now possible and requires the same precision in the description of the physics of their interiors.

It has been recently emphasized that difficulties arise when trying to fit observed and computed main-sequences, as models look hotter than the real objects (Baglin 1997; Lebreton et al. 1997; Cayrel et al. 1997; Lebreton et al. 1998).

Several effects can been advocated to explain this discrepancy, as for instance, the treatment of the superadiabatic outer layers or observational bias due to NLTE effects, in the effective temperature scale and in the abundance determinations (Thevenin & Idiart 1999).

We propose in this paper to document the role of microscopic diffusion in these stages of evolution, and to quantify its influence on the global parameters of these stars and on their position in the HR diagram.

It is well known that, on the main-sequence, variations of helium Y and of the metal content Z act in opposite directions: while decreasing Y reduces the effective temperature $T_{\rm eff}$ and the luminosity L, a decrease of the metal content increases both L and $T_{\rm eff}$. Microscopic diffusion, which acts on both Y and Z, creates a stratification of chemicals in radiative zones. The global effects on the observables i.e. the modification of the HR diagram position, but also the changes of the surface metal

Table 1. [Fe/H] and initial abundances, per mass unit, of hydrogen X and heavy elements Z.

Labels	[Fe/H]	X	Z
07	−0.75	0.7544	0.0056
09	−0.94	0.7564	0.0036
12	−1.24	0.7582	0.0018
17	−1.72	0.7594	0.0006

abundance, are quite subtle; they have to be taken into account altogether to perform a precise comparison with observations.

The paper is organized as follows: the set of stellar models is listed in Sect. 2, whereas the input physics is described in Sect. 3. The effects of microscopic diffusion on the evolution of subdwarfs are presented in Sect. 4, the "calibration" procedure needed when comparing theoretical predictions and observations is developped in Sect. 5, whereas the influence on the HR diagram and on the shape of the isochrones as a function of their present observed metal content is described in Sect. 6. Future prospects and possible tests of this hypothesis are suggested in Sect. 7.

2. The stellar models

As subdwarfs belong to population II, their initial helium content is close to the primeval value. Then stellar models depend only on age and metal content, assuming that the physical description is completely settled.

In old metal poor stars, α elements enrichment seems to be always present (see e.g. Wheeler et al. 1989), though large variations exist from one star to the other. We have used in all our models the mixture of Allard (1996) with the α-enrichment relative to the Sun, $[\alpha/\mathrm{Fe}] = 0.3$. Four initial metal contents, represented by the standard [Fe/H] observable, have been considered: $[\mathrm{Fe/H}] \sim -0.75,\ -0.94,\ -1.24$ and -1.72. The initial total amount of helium, i.e. $^3\mathrm{He} + {}^4\mathrm{He}$, per mass is fixed to its primordial value assumed to be $\mathrm{Y} = 0.24$ (Izotov et al. 1997). With respectively $\mathrm{Z_{Fe}}$, X and Z as the iron, hydrogen and heavy elements mass ratio, we use the relation:

$$[\mathrm{Fe/H}] \equiv \log(\mathrm{Z_{Fe}/Z}) + \log(\mathrm{Z/X}) - \log(\mathrm{Z_{Fe}/X})_\odot \qquad (1)$$

to relate the observed metallicity and metal content. Here $\log(\mathrm{Z_{Fe}/X})_\odot \equiv -2.753$ for the solar mixture of Grevesse & Noels, (1993), and and $\log(\mathrm{Z_{Fe}/Z}) \equiv -1.371$ for the Allard's α-enriched mixture.

The initial mass ratio X and Z are derived from the initial values of Y and [Fe/H] as given in Table 1.

To describe the lower part of the main-sequence we present here models of masses varying from 0.6 to $0.85 M_\odot$ evolving up to 10 Gy. Below $0.6 M_\odot$, evolution is extremely slow, and above $0.85 M_\odot$ subdwarfs have left the main-sequence. As during the rapid pre main-sequence phase, the stellar models are almost fully mixed by convection, the microscopic diffusion is inefficient, and starting the computations at the homogeneous main-sequence stage is sufficient for our purpose.

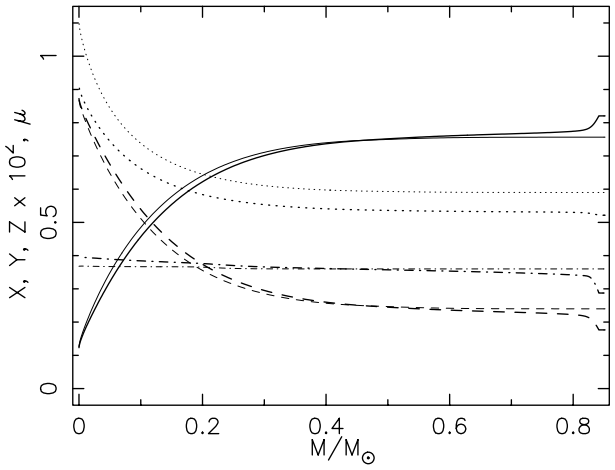

Fig. 1. Profiles of abundances, in mass, of hydrogen X (full), helium Y (dash), heavy elements Z (dot-dash) and mean molecular weight μ (dot) for two $0.85 M_\odot$ models evolved up to 10 Gy, respectively with (heavy) and without (thin) microscopic diffusion.

3. Physics of stellar models

Nuclear network and chemical mixture. The general nuclear network we used contains the following species: $^1\mathrm{H}$, $^3\mathrm{He}$, $^4\mathrm{He}$, $^{12}\mathrm{C}$, $^{13}\mathrm{C}$, $^{14}\mathrm{N}$, $^{15}\mathrm{N}$, $^{16}\mathrm{O}$, $^{17}\mathrm{O}$, and Ex. Ex is a fictitious mean non-CNO heavy element with atomic mass 28 and charge 13, which complements the mixture. With respect to time, due to the diffusion processes, the abundances of heavy elements are enhanced toward the center; Ex mimicks that enhancement for the non CNO metals which contribute to changes of Z, then to opacity variations. We have taken into account the most important nuclear reactions of PP+CNO cycles (Clayton, 1968) with the species $^2\mathrm{H}$, $^7\mathrm{Li}$, $^7\mathrm{Be}$ at equilibrium. The relevant nuclear reaction rates are taken from Caughlan and Fowler (1988); weak screening is assumed.

For helium the initial isotopic ratio is fixed at $^3\mathrm{He}/^4\mathrm{He} = 4.19\,10^{-4}$ (Gautier & Morel 1997). In the mixture of heavy elements, the ratios between the CNO species are set to their α-enriched Allard (1996) values (in number) C: 0.147909, N: 0.038904 and O: 0.616594, with the isotopic ratios: $^{13}\mathrm{C}/^{12}\mathrm{C} = 1.11\,10^{-3}$, $^{15}\mathrm{N}/^{14}\mathrm{N} = 4.25\,10^{-3}$, $^{17}\mathrm{O}/^{16}\mathrm{O} = 3.81\,10^{-4}$ (Anders & Grevesse, 1989).

Diffusion. Different processes are participating to element separation or mixing. Whereas gravitational settling creates stratification, hydrodynamical instabilities can, at least in some phases of evolution, generate macroscopic motions which tend to reduce the chemical inhomogeneities. Presently, no general description exists of these processes, which could be easily incorporated in stellar evolution calculations. As the purpose of this paper is to evaluate the influence of elements segregation in comparing theory and observations of subdwarfs, we did not take into account any of these processes. Let us note that rotation, which has been identified as one major cause of partial mixing is almost absent in these old low mass objects.

Microscopic diffusion is described using the formalism of Michaud & Proffitt (1993) valid for main-sequence stars. The radiative forces are not taken into account. For Y the mass conservation equation gives: $V_Y = -\mathrm{X}V_X/\mathrm{Y}$ where the original equation has been slightly modified to take into account the heavy elements; V_X and V_Y are respectively the diffusion velocities of hydrogen and helium. This description is parameter free, depending only on known coefficients. A more complete discussion of the method used to treat diffusion is given in Morel et al. (1997).

Equation of state and Opacities. We have used the EFF equation of state (Eggleton et al. 1973) sufficient for our purpose in this mass range.

We have chosen the Livermore Library (Iglesias & Rogers 1996) with the α-enriched mixture of Allard (1996), complemented at low temperature opacities by the Kurucz's (1998) α-enriched tables. Unfortunately there is no available common mixture in these libraries; we have retained the closest ones with a rough smoothing in the extreme low temperature atmospheric layers.

The opacities and equation of state are functions of the heavy elements content Z, through the number of free electrons and the abundances of efficient absorbers which do not necessarily belong to the nuclear network e.g. ^{56}Fe. Due to diffusion and nuclear reactions, Z changes as the star evolves, as well as the ratios between the abundances of chemicals. In the calculation of opacities and equation of state, Z is separated in two parts: the first one consists of the chemicals heavier than helium which, belonging to the CNO nuclear network, are both diffused and nuclearly processed; Ex, the second part, is only diffused. Hence in the estimate of Z, the changes of CNO abundances caused by diffusion, nuclear processes and the effects of the gravitational settling of the heaviest non-CNO species are taken into account.

Convection. In the convection zones the temperature gradient is computed according to the standard mixing-length theory, with the mixing-length defined as $l \equiv \lambda H_{\mathrm{p}}$, where H_{p} is the classical pressure scale height. The constancy of λ has been demonstrated for population I models close to the main-sequence (see e.g. Fernandes et al. 1998), and calibrations of λ from 2D simulations (Ludwig et al. 1998) lead to approximately the same result; so, we assume that λ is constant and equal to the value obtained for a solar model using the same physics, namely $\lambda \equiv 1.7$. This hypothesis has no influence on the results of this paper devoted to an estimate of the differential effect of microscopic diffusion.

In the models with diffusion the convection zones are mixed via a strong turbulent diffusion coefficient, which produces an homogeneous composition.

Atmosphere. An atmosphere is restored using the Hopf's $T(\tau)$ law: $T^4 = \frac{3}{4}T_{\mathrm{eff}}^4[\tau + q(\tau)]$ (Mihalas 1978) with τ as the Rosseland optical depth. The connection with the envelope is made at the optical depth $\tau_{\mathrm{b}} = 10$, where the diffusion approximation for radiative transfer becomes valid. In the convective part of the atmosphere, a numerical trick (Henyey et al. 1965) is employed in connection with the purely radiative Hopf's law in order to ensure the continuity of gradients at the limit between the atmosphere and the envelope. At each time step, the radius $R_\star$ of the model is taken at the optical depth $\tau_\star \simeq 0.6454$ where $T(\tau_\star) = T_{\mathrm{eff}}$; the mass of the star $M_\star$, is the mass inside the sphere of radius $R_\star$. The external boundary is fixed at the optical depth $\tau_{\mathrm{ext}} = 10^{-4}$, where a boundary condition on the pressure is expressed as: $P(\tau_{\mathrm{ext}}) = g \,/\, \kappa\tau_{\mathrm{ext}}$, with g as the gravity and κ as the Rosseland mean opacity.

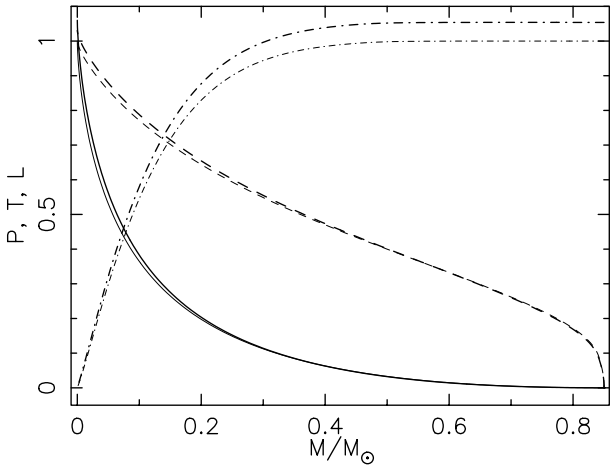

Fig. 2. The same, see Fig. 1, for normalized pressure (full), temperature (dash) and luminosity (dot-dash). The factors of normalization are respectively $4.7\,10^{17}$ dyne cm^{-2} for the pressure, $1.7\,10^{7}$ K for the temperature and $3.6\,10^{33}$ erg cm^{-2} s^{-1} for the luminosity.

Numerics. The models have been computed using the CESAM code (Morel 1997). Typically each evolutionary track needs of the order of 85 models of about 500 mass shells. The accuracy of the numerical scheme is one for the time and three for the space.

4. Effects of microscopic diffusion on the structure of main-sequence models

Due to the gravitational settling, all species but ^{1}H sink; therefore as time goes on, the amount of hydrogen at the surface is enhanced while the amount of helium and heavy elements decreases. Then a first effect of microscopic diffusion is the decrease of the surface value of [Fe/H] with respect to time. The variation of Z modifies the opacity and then changes slightly the temperature gradient in the radiative zones, as well as the position of their boundaries.

In the mean time, the sinking of helium with respect to hydrogen produces a decrease of the mean molecular weight μ in the envelope as, assuming here a complete ionisation:

$$\mu \simeq \left(2\mathrm{X} + \frac{3}{4}\mathrm{Y} + \frac{\mathrm{Z}}{2}\right)^{-1} \text{ and } d\mu \simeq -\mu^2\left(\frac{5}{4}dX + \frac{dZ}{2}\right).$$

In the outer layers of a model computed with microscopic diffusion $dX \geq 0$, $dY \leq 0$ and $dZ \leq 0$ then $d\mu < 0$ as Z $\ll$ X, see Fig. 1.

This variation of the mean molecular weight produces an increase of the radius and consequently a decrease of the effective temperature. But, the variation of the metal content introduces a concomitant variation of the opacity in the radiative regions, which tends to counterbalance this effect.

With the initial abundances given in Table 1, we have computed respectively sets of models, i) without diffusion, ii) with diffusion of helium only, iii) with diffusion of all species.

The main characteristics of four models of masses $0.85M_{\odot}$, $0.8M_{\odot}$ and $0.75M_{\odot}$, at the age of 10 Gyr computed without and with microscopic diffusion of all species are displayed in Table 2 and in Table 3 for the models of $0.7M_{\odot}$ and $0.6M_{\odot}$[1].

During the main-sequence, models with diffusion are cooler than models without diffusion; this is essentially due to the changes of the mean molecular weight. As already stressed by Castellani et al. (1997) comparison with unphysical models, including diffusion of helium only, shows that a significant contribution to the displacement in the HR diagram is due to helium settling, in particular for low metal content as illustrated on Fig. 3.

In the following, we will call "diffusion shift" **DS**, the translation in the HR diagram from a "standard model" to a model including microscopic diffusion, at the *same mass and the same age*. It consists in:

- a reduction of the effective temperature, decreasing with mass from 100 K at $0.85M_{\odot}$, to almost zero at $0.6M_{\odot}$; the stronger increase when [Fe/H] decreases is explained by the larger influence of helium stratification at low metallicities;
- an augmentation of the luminosity of the order of 0.01 to 0.02 dex, almost independent of [Fe/H], very sightly decreasing with mass, almost certainly due to the higher temperature and higher helium content of the central core of models with diffusion.

The time dependence of the process shows up through the increasing separation between the tracks as evolution proceeds.

5. "Calibration" of the subdwarfs main-sequence

Due to the decrease of the surface value of [Fe/H] along the evolution, the stars presently observed with a given $[\mathrm{Fe/H}]_{\star}$ have started their evolution with a larger $[\mathrm{Fe/H}]_0$ value of their metal content.

To represent observed data, models have then to be "calibrated" to reach the observed surface $[\mathrm{Fe/H}]_{\star}$ value at their present age. Assuming a linear dependence $\Delta[\mathrm{Fe/H}]/[\mathrm{Fe/H}]$ with respect to mass and age, for a given mass and a given age, one can estimate the initial $[\mathrm{Fe/H}]_0$ needed to reach the observed value, and start again a new evolutionary sequence including diffusion. If needed, this process can be iterated.

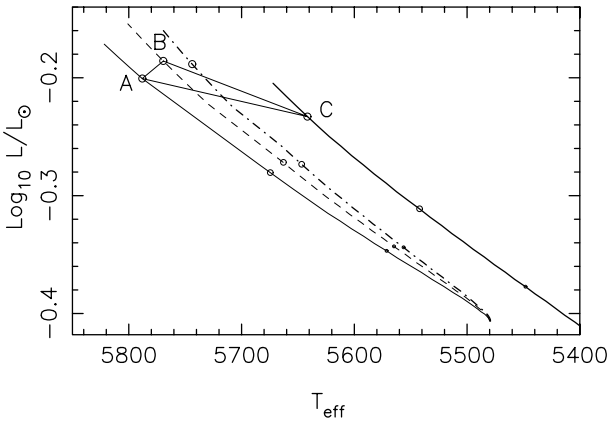

Fig. 3. The main-sequence HR evolutionary tracks for $0.8M_{\odot}$, $[\mathrm{Fe/H}] = -0.94$, without diffusion (thin full), with diffusion of helium only (dash-dot-dash), with diffusion of all elements (dashed), and finally with the calibration of surface [Fe/H] (heavy full) (the initial metallicity has been computed in order to achieve, at 10 Gyr, the initial surface metallicity of the other three models). On each evolutionary track the open circles correspond to ages of 3 Gy, 6 Gy and 9 Gy respectively. For 9 Gy, AB is the diffusion shift **DS**, BC the calibration shift **CS** and AC the global shift **GS** (see text).

This effect adds a new shift of the HR position of the models towards the red, called the "calibration shift" **CS**, see Fig. 3. It also increases with age, as it is due to a reduction of the surface abundances as evolution proceeds. It consists in:

- a decrease of the effective temperature due to the higher initial metal content, which is higher for higher metal content and decreases with mass from 140 K at $0.85M_{\odot}$, to 30 K at $0.6M_{\odot}$, for $[\mathrm{Fe/H}] = -0.94$.
- a reduction of the luminosity, strongly depending on mass and becoming very small for $0.6M_{\odot}$, which is also due to the higher metal content.

The extend of **CS** depends on the relative variation of $[\mathrm{Fe/H}]$ during the evolution, as seen from Table 2 and 3 where are displayed the main characteristics of the models with enhanced initial $[\mathrm{Fe/H}]_0$ (label "dc") in order to obtain at the end of the evolution, the surface values of $[\mathrm{Fe/H}]_{\star}$ close to the values of Table 1.

6. The global shift

We will call "global shift" **GS**, the combined effect of diffusion and calibration. Its component in effective temperature is given in Table 2 and 3 for the 10 Gy models. Fig. 6 shows, as a function of mass, the variations of effective temperature for the three different metal content considered here.

Both diffusion and calibration reduce the effective temperature, but in an opposite way with respect to [Fe/H]. The effect of diffusion increases while the effect of calibration decreases with [Fe/H].

[1] There, for the calculations of [Fe/H] with Eq. (1), the differential changes between Z_{Fe} and Z, due to gravitational settling and radiative forces, which act on opposite way, are neglected and $\log(Z_{Fe}/Z) \equiv -1.371$ is used.

Table 2. Characteristic of models of $0.85M_\odot$ (Q), $0.80M_\odot$ (N), $0.75M_\odot$ (R), $0.70M_\odot$ (P) and $0.60M_\odot$ (S) at 10Gy. The models evolved with microscopic diffusion are specified by the labels 'dc' and 'd' respectively for calibrated and non-calibrated (see text). $M_{\rm bol}$ is the bolometric magnitude, ($M_{\odot\,\rm bol} \equiv 4.75$); $\rm X_\star$ and $\rm Y_\star$ are respectively the surface abundances, in mass unit, of hydrogen and helium; $\rm X_0$ and $\rm Z_0$ are respectively the initial surface abundances, in mass unit, of hydrogen and heavy elements of calibrated models "dc"; $[\rm Fe/H]_0$ and $[\rm Fe/H]_\star$ are respectively the surface values of [Fe/H] at zero age main-sequence and at 10Gy; $\rm GS_T$ in Kelvin, is the component on the $T_{\rm eff}$ axis of the global shift **GS** (see text) for 10 Gy.

	Q07	Q09	Q12	Q17	N07	N09	N12	N17	R07	R09	R12	R17
$T_{\rm eff}$	5832	6097	6401	6720	5545	5822	6144	6430	5222	5500	5832	6116
$M_{\rm bol}$	4.972	4.649	4.243	3.811	5.447	5.179	4.869	4.573	5.903	5.664	5.398	5.163
	Q07d	Q09d	Q12d	Q17d	N07d	N09d	N12d	N17d	R07d	R09d	R12d	R17d
$T_{\rm eff}$	5809	6060	6322	6584	5531	5801	6101	6363	5215	5488	5810	6080
$M_{\rm bol}$	4.925	4.592	4.174	3.702	5.408	5.136	4.818	4.510	5.869	5.628	5.358	5.119
$\rm X_\star$	0.802	0.821	0.853	0.880	0.795	0.807	0.825	0.859	0.789	0.797	0.808	0.825
$\rm Y_\star$	0.192	0.177	0.146	0.120	0.200	0.190	0.174	0.141	0.206	0.200	0.190	0.175
$[\rm Fe/H]_\star$	-0.85	-1.07	-1.45	-2.00	-0.83	-1.04	-1.38	-1.94	-0.82	-1.02	-1.35	-1.86
	Q07dc	Q09dc	Q12dc	Q17dc	N07dc	N09dc	N12dc	N17dc	R07dc	R09dc	R12dc	R17dc
$\rm X_0$	0.753	0.755	0.757	0.759	0.753	0.756	0.758	0.759	0.753	0.756	0.757	0.759
$\rm Z_0$	0.007	0.005	0.003	0.001	0.007	0.005	0.002	0.001	0.007	0.004	0.002	0.001
$T_{\rm eff}$	5674	5920	6202	6477	5415	5672	5999	6293	5117	5405	5751	6054
$M_{\rm bol}$	5.077	4.779	4.382	3.892	5.519	5.262	4.937	4.590	5.955	5.698	5.412	5.144
$\rm X_\star$	0.797	0.811	0.835	0.872	0.791	0.801	0.816	0.849	0.786	0.795	0.805	0.822
$\rm Y_\star$	0.197	0.185	0.163	0.128	0.203	0.195	0.182	0.151	0.208	0.201	0.193	0.117
$[\rm Fe/H]_0$	-0.66	-0.82	-1.08	-1.50	-0.67	-0.84	-1.12	-1.56	-0.68	-0.88	-1.17	-1.65
$[\rm Fe/H]_\star$	-0.75	-0.94	-1.25	-1.76	-0.75	-0.94	-1.24	-1.76	-0.75	-0.96	-1.27	-1.78
$\rm GS_T$	-158	-177	-199	-243	-130	-150	-145	-137	-105	-95	-81	-62

Table 3. Same as Table 2 for models of $0.70M_\odot$ (P) and $0.60M_\odot$ (S).

	P07	P09	P12	P17	S07	S09	S12	S17
$T_{\rm eff}$	4885	5146	5473	5774	4275	4453	4699	4983
$M_{\rm bol}$	6.354	6.137	5.895	5.688	7.264	7.087	6.883	6.701
	P07d	P09d	P12d	P17d	S07d	S09d	S12d	S17d
$T_{\rm eff}$	4880	5139	5461	5756	4277	4453	4699	4983
$M_{\rm bol}$	6.325	6.105	5.861	5.653	7.239	7.061	6.856	6.673
$\rm X_\star$	0.784	0.791	0.798	0.807	0.776	0.782	0.786	0.789
$\rm Y_\star$	0.211	0.206	0.200	0.193	0.218	0.215	0.212	0.211
$[\rm Fe/H]_\star$	-0.81	-1.01	-1.32	-1.82	-0.79	-0.99	-1.30	-1.78
	P07dc	P09dc	P12dc	P17dc	S07dc	S09dc	S12dc	S17dc
$\rm X_0$	0.754	0.755	0.758	0.759	0.753	0.756	0.758	0.759
$\rm Z_0$	0.006	0.004	0.002	0.001	0.006	0.004	0.002	0.001
$T_{\rm eff}$	4803	5072	5413	5742	4239	4420	4672	4979
$M_{\rm bol}$	6.394	6.159	5.898	5.664	7.280	7.092	6.876	6.675
$\rm X_\star$	0.782	0.789	0.797	0.806	0.775	0.781	0.785	0.789
$\rm Y_\star$	0.212	0.207	0.201	0.194	0.219	0.216	0.213	0.211
$[\rm Fe/H]_0$	-0.69	-0.89	-1.19	-1.68	-0.71	-0.90	-1.21	-1.71
$[\rm Fe/H]_\star$	-0.75	-0.96	-1.27	-1.78	-0.75	-0.95	-1.26	-1.77
$\rm GS_T$	-83	-74	-60	-32	-36	-33	-27	-4

In luminosity the situation is different. The calibration procedure compensates partly the luminosity increase due to diffusion. The variation can reach 0.03 dex, depending both on mass and [Fe/H]. The mass dependence remains strong, from 0.06 dex at $0.85M_\odot$, to 0.01 dex at $0.6M_\odot$. It produces a distortion in the Mass-Luminosity relation, see Fig. 7, depending on [Fe/H], an effect which could be detected with high quality data on a reasonable set of objects.

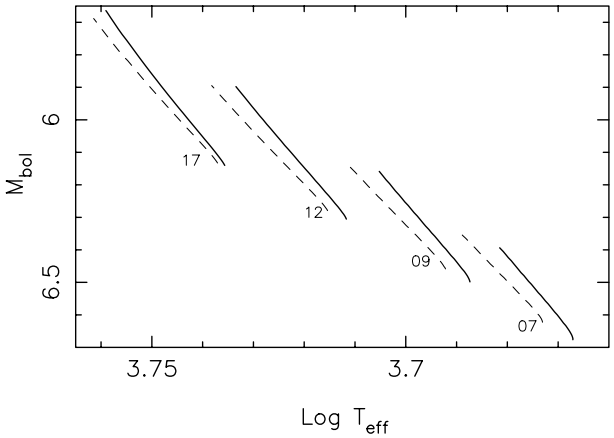

Fig. 4. The main-sequence evolutionary tracks of $0.7\,M_\odot$ models, evolved without diffusion (dashed) and calibrated (full). The solar bolometric magnitude is taken as $M_{\odot\,\mathrm{bol}} \equiv 4.75$.

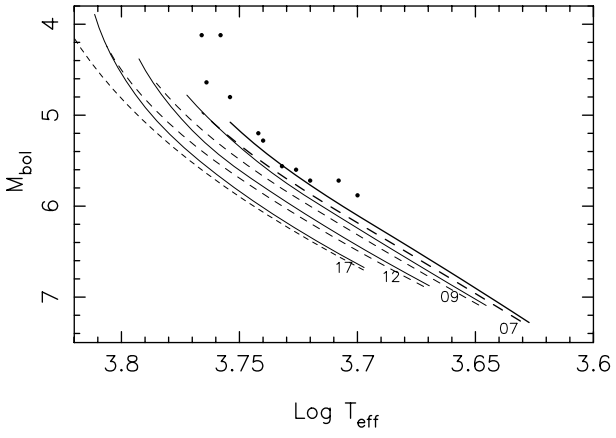

Fig. 5. Schematic isochrones at 10 Gy for models with $[\mathrm{Fe/H}]_\star = -0.75,\ -0.94,\ -1.24$ and -1.72; dashed: model without diffusion, full: calibrated models with diffusion. •: locations of stars with observed [Fe/H] within $-1.0 < [\mathrm{Fe/H}] < -0.45$ as derived from Hipparcos data.

The displacement in the HR diagram is seen as a translation towards lower effective temperatures, see Fig. 4. It produces a slight variation of the curvature of the evolutionary track, see Fig. 5, due to the time dependence of the process. Isochrones are then slightly more vertical.

Stars with observed [Fe/H] within $-1.0 < [\mathrm{Fe/H}] < -0.45$ and the most accurate fundamental parameters, studied by Lebreton et al. (1997) have been added to Fig. 5. As already said, though microscopic diffusion tends to reduce the discrepancy between the effective temperature of observed and theoretical models, the effect is not sufficient to solve the difficulty.

For $[\mathrm{Fe/H}] = -1.72$, Fig. 8 shows, as a function of luminosity and effective temperature, the effective temperature difference between two isochrones at the same luminosity: the standard one experiences no diffusion and its initial abundances are equal to the observed ones, while the second one is computed using our proposed calibration.

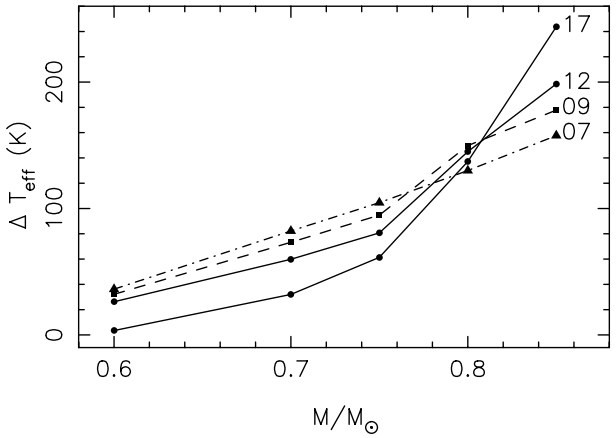

Fig. 6. Total variation of effective temperature at 10 Gy between standard and calibrated models with respect to the mass. At $0.85\,M_\odot$ evolutionary effects become significant.

7. Discussion

We have estimated in this paper the influence of gravitational and thermal settling, on the global parameters of low main-sequence stars. As we have introduced only microscopic flows in the computations except in convective zones, the stratification is probably overestimated.

We have shown that this physical process, if at work permanently, produces an effective temperature shift towards the red. For population II stars it exceeds generally 100 K.

Compared to the most reliable data available at present, the predicted shift is of the right order of magnitude, but probably slighly unsufficient to eliminate completely the discrepancy shown by Lebreton et al. (1997). However, as already mentioned, other effects could also be responsible for redshifts of that kind. So that more precise characteristic behaviors are needed to decipher among the different possibilities. Let us cite a few signatures of the microscopic diffusion.

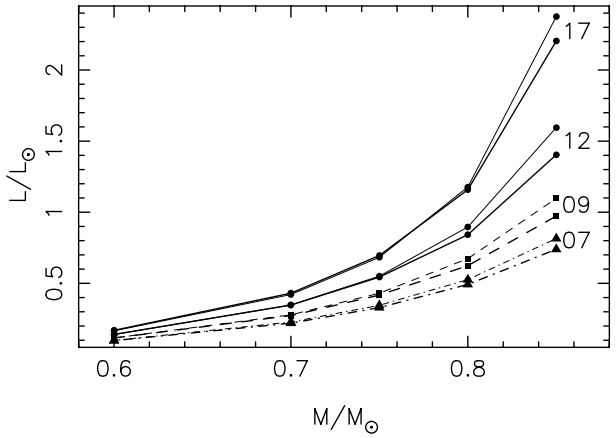

Fig. 7. Mass-luminosity diagram at 10 Gy for standard (thin) and calibrated (thick) models.

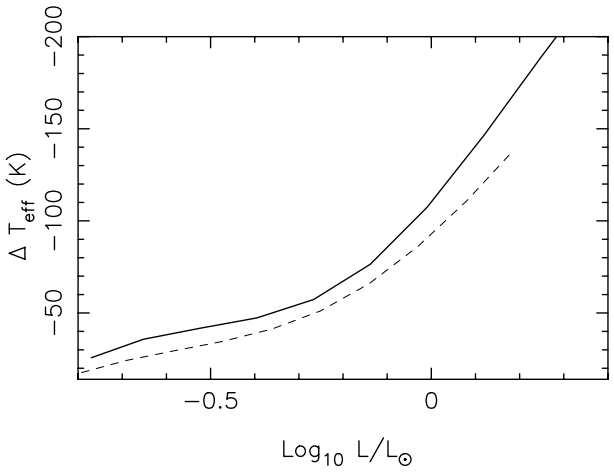

Fig. 8. Temperature difference between two isochrones at the same luminosity as a function of luminosity, respectively for 10 Gy (full) and 8 Gy (dahed), with $[\mathrm{Fe/H}]_\star = -1.72$ – wigles are due to the interpolation procedure.

- the predicted shift increases with age and decreases when [Fe/H] increases;
- the mass-luminosity relationship is modified depending on Z as at a given mass and age, as diffused and calibrated models are less luminous than standard ones;
- the slope of isochrones is slightly increased.

Though very important improvement on the quality of the observational data on the nearest members of the old population have been obtained recently, they remain too coarse and too few to allow unambiguous tests. More objects with accurate fundamental parameters are needed to validate definitely this hypothesis.

A lot of progress is expected from the GAIA mission (Perryman et al. 1997), which will provide even more accurate distances and sometimes masses for a larger number of stars. But improvements in the determination of atmospheric parameters, as well as in methods of comparing observed and predicted quantities are also badly needed.

Acknowledgements. We are grateful to G. Alecian, Y. Lebreton and R. Cayrel for helpful discussions and communicating their work before publication. We would also like to thank the referees, Drs. S. Degl'Innocenti and Dr. V. Castellani, for their careful review of this paper and for a number and useful suggestions. This work was partly supported by the GDR G131 "Structure Interne des Etoiles et des Planètes géantes" of CNRS (France). Most of this work has been performed using the computing facilities provided by the OCA program "Simulations Interactives et Visualisation en Astronomie et Mécanique (SIVAM)".

References

Allard F., 1996, cited as a private communication on the WEb site http://www-phys.llnl.gov/V_Div/OPAL
Alonso A., Arribas S., Martines-Roger C., 1996, A&AS 117, 227
Anders E., Grevesse N., 1989, Geochimica et Cosmochimica Acta 53, 197
Baglin A., 1997, Hipparcos and the theory of stellar interiors: what has been learned? In: Turon C. (ed.) IAU GA, Kyoto JD 14, Highlights in Astronomy. In press
Basu S., 1997, The seismic Sun. In: Provost J., Schmider F.X. (eds.) IAU symposium No. 181, Sounding solar and stellar interiors. Kluwer, 137
Brun S., Turck-Chièze S., Morel P., 1998, ApJ 506, 913
Caughlan G.R., Fowler W.A., 1988, Atomic Data and Nuclear Data Tables 40, 284
Cayrel R., Lebreton Y., Perrin M-N., et al., 1997, The HR diagram of pop II stars with Hipparcos parallaxes. In: Perryman M.A.C., Bernacca P.L. (eds.) Hipparcos Venice 97, ESA SP-402, 219
Chaboyer B., Sarajedini A., Demarque P., 1992, ApJ 394, 515
Castellani V., Ciacio F., Degl'Innocenti S., Fiorantini S., 1997, A&A 322, 801
Christensen-Dalsgaard J., Däppen W., Antia H.M., et al., 1996, Science 272, 1286
Clayton D.D., 1968, Principles of Stellar Evolution and Nucleosynthesis. Mc Graw–Hill
Eggleton P.P., Faulkner J., Flannery B.P., 1973, A&A 23, 325
Fernandes J., Lebreton Y., Baglin A., Morel P., 1998, A&A 338, 455
Gough D.O., Kosovichev A.G., Toomre J., et al., 1996, Science 272, 1296
Gautier D., Morel P., 1997, A&A 323, L9
Grevesse N., Noels A., 1993, Cosmic Abundances of the Elements. In: Prantzos N., Vangioni-Flam E., Casse M. (eds.) Origin and Evolution of the Elements. Cambridge University Press, 14
Henyey L., Vardya M., Bodenheimer P., 1965, ApJ 142, 841
Hui Bon Hoa A., Alecian G., 1998, A&A 332, 224
Iglesias C.A., Rogers F.J., 1996, ApJ 464, 943
Izotov Y.I., Thuan T.X., Lipovetsky, V.A., 1997, ApJS 108, 1
Kurucz R., 1998, taken from the WEb site http://cfaku5.harvard.edu/OPACITIES
Lebreton Y., Perrin M-N., Fernandes J., Cayrel R., Cayrel de Strobel G., Baglin A., 1997, The H-R Diagram for Late-Type Nearby Stars as a Function of Helium Content and Metallicity. In: Perryman M.A.C., Bernacca P.L. (eds.) Hipparcos Venice 97, ESA SP-402, 379
Lebreton Y., Perrin M-N., Cayrel R., Baglin A., Fernandes J., 1998, A&A, in press
Ludwig H.G., Freytag B., Steffen M., A&A submitted
Mazzitelli I., d'Antona F., Caloi V., 1995, A&A 302, 382
Michaud G., Proffitt C.R., 1993, Particule Transport Process. In: Baglin A., Weiss W.W. (eds.) Inside the Stars, IAU Colloquium 137, ASP Conference Series, Vol. 40, 246
Mihalas D., 1978, Stellar Atmosphere, 2d. Ed., Freeman and Cie
Morel P., 1997, A&AS 124, 597
Morel P., Provost J., Berthomieu G., 1997, A&A 327, 349
Perryman M.A.C., Bernacca P.L., 1997, Hipparcos Venice 97, ESA SP-402, 410
Perryman M.A.C., Lindengren L., Turon C., 1997, The scientific goals of the GAIA mission, In: Perryman M.A.C., Bernacca P.L. (eds.) Hipparcos Venice 97, ESA SP-402, 743
Richard O., Vauclair S., Charbonnel C., Dziembowsky D.A., 1996, A&A 312, 1000
Thevenin F., Idiart T., 1999, ApJ, submitted
Vauclair S., Charbonnel C., 1998, ApJ, in press
Wheeler J.C., Sneden C., Truran J.W., 1989, ARA&A 27, 279